

Article

Satellite Assessments of Tropopause Dry Intrusions Correlated to Mid-Latitude Storms

Yi-Xuan Shou ^{1,*}, Feng Lu ¹ and Shaowen Shou ²

¹ Key Laboratory of Radiometric Calibration and Validation for Environmental Satellites, National Satellite Meteorological Center, China Meteorological Administration, Beijing 100081, China; lufeng@cma.gov.cn

² Department of Atmosphere, Nanjing University of Information Science & Technology, Nanjing 210044, China; sshou999@126.com

* Correspondence: yshou@atmos.umd.edu or shouyx@cma.gov.cn; Tel.: +301-273-5507

Academic Editor: Robert W. Talbot

Received: 2 August 2016; Accepted: 1 October 2016; Published: 11 October 2016

Abstract: Dry intrusion is an important mid-latitude atmosphere phenomenon within the upper troposphere and lower stratosphere. It is often found to be related to the cyclogenesis, rainstorm, as well as convection generation and precipitation enhancement. Since the atmosphere environment for any of these above-mentioned weather is terribly complicated, those preexisting popular schemes which takes no account of water vapor may not suitable for detecting the dry intrusion related to such weather events. With regard to the merits and demerits of the current preexisting schemes, a new scheme based on Fengyun-2E geo-stationary satellite data is presented in this study to detect the tropopause dry intrusion. The scheme is set up based on the statistical relationship between water vapor at high level troposphere, the general moist potential vorticity, ozone concentration and upper-level jets. Validations are made by using Fengyun-3B observed ozone profiles and NCEP FNL analysis data. Two mid-latitude storm episodes occurred in China in 2012 and 2014 are selected as demonstration to show the applicability of the method we developed in this study. Good application effects in both cases suggest that the new method for detecting dry intrusion is applicable and can be helpful in middle-latitude disastrous weather monitoring and forecasting.

Keywords: dry intrusion; stratosphere-troposphere exchange; mid-latitude; satellite

1. Introduction

Stratosphere-troposphere exchange is always described as a dynamical, chemical and radiative coupling process of the material of the two lowest layers of the atmosphere. Their crucial interplay with convection and transport of the chemical materials has therefore attracted widespread attention in the research community since it is first found by Reed in 1955 [1]. The process of air mass passively moving from stratosphere to troposphere is always called as tropopause folding or dry intrusion since the air mass within stratosphere is relatively dry and has a high potential vorticity value and ozone concentration. As documented by the previous studies, the intensity and evolution of dry intrusion can be treated as important indices in forecasting the severe weather over mid-latitude region since it suggests frontogenesis at upper level which will impact on the development of convective cloud and the further convection [1]. To precisely estimate the intensity and predict the evolution of the dry intrusion, so far several methods based on diagnosis and modeling or their combinations are developed.

The diagnosis method can be further divided into two categories with one that based mainly on the conventional observations (such as, rawinsonde, radiosonde etc.) and the other that on the basis of remote sensing techniques. Since the former diagnosis method is always limited by the temporal and spatial resolution, it has been rarely used directly for estimation nowadays but for

validation instead [2–4]. Since 1960 when the first weather satellite was successfully launched, satellite observations are used widespread in various perspectives. Among them the upper atmospheric study is found to be benefit from satellites over the rest fields due to their top-down view angle characteristics and some specific properties of their channels. As for the dry intrusion, it is often found in the water vapor (WV) channels of weather satellite due to the sensitivity of the irradiance of these channels to the water content over the upper troposphere [5]. For example, the peak value of the weight functions of the WV channel (the center wavelength is of 6.7 μm) of Fengyun-2E geostationary weather satellite is located around 400 hPa which means air parcels with low moisture will hardly be seen by this channel of the satellite. On the satellite images, these areas will be shown as some dark areas with high brightness temperature. Based on this property, the second diagnosis method of dry intrusion that based on the given brightness temperature of the WV channels is developed. Due to its ease of implementation and having a relatively high consequence on temporal and spatial scales, this method is currently used more often. While one may find that a numerous of erroneous or missed detections may occur by merely using a simple threshold value. For example, the dark areas on the WV channel images are always observed over the Sahara, Indian and Arabian deserts around the Tropic of Cancer. While they are formed due to the low moisture content within the whole atmospheric column over these areas other than the tropopause dry intrusion. On the other hand, some intense dry intrusions that occurred over the high latitude areas may have a relatively low brightness temperature or show brighter on the cloud images than that observed over the low latitude areas due to the lower temperature. In such situation, the interface between the dry and moisture air is often blurred and hard to be detected. Besides, it was documented by Roger and Holmes [5], seasonal variation could also be a factor which would impact the accuracy of the dry intrusion detection on satellite images. Therefore, the diagnosis based on brightness temperature of WV channels is also not an optimized method for detecting dry intrusion in atmosphere.

Numerical modeling is another popular method that used for detecting dry intrusion. It is developed with the development of high-resolution numerical models [6]. This method is better than the diagnosis that based on conventional observations due to its high spatial and temporal resolution. But sometimes scientists find the the existence of some modeling dry intrusions cannot be proven by observations [7,8]. For example, Bithell et al. [7] once documented that the lower-level intrusions could be found in the simulations but may not be visible in the satellite or ground-based observations.

Considering the pros and cons, a combination of the diagnosis on the basis of remote sensing techniques and modeling is developed. The main idea of this method is based on the property of the WV channel as well as dynamics and thermodynamics of the dry intrusion extracted from numerical modeling data. It is first set up by Wimmers et al. [9–11] and Michel [12,13]. The method proposed by Wimmers et al. is tested with GOES (geostationary operational environmental satellite) geostationary satellite data and National Centers for Environmental Prediction (NCEP) Global Forecast System (GFS) numerical forecasting by considering the relation between the dry intrusion and moisture. While, Michel's method is set up based on the relation between the dry intrusion and potential vorticity (PV) and is tested with MSG (Meteosat Second Generation) geostationary satellite and European Center for Medium range Weather Forecasting (ECMWF) data. Although both of them are proven to be optimized than the previous methods, it is found that their methods are based on the hypothesis that the dry intrusion is occurred under a complete dry atmosphere circumstance. So that the diabatic heating is ignored in the calculation of the physics parameters related to the dry intrusions in their methods. This hypothesis is often found to be questionable for the dry intrusions associated with rainstorms and some other severe convective weather due to the non-saturation state of air parcels under these circumstances.

Therefore, an improved combination method based on satellite and numerical forecasting for detecting dry intrusions associated severe convective weather is developed in this study. It will be tested with Fengyun-2 geostationary satellite and NCEP/GFS numerical data. This paper is organized as follows. In Section 2, the new method raised in this study is briefly described. And a validation and

two mid-latitude storm episodes are used to evaluate the new method in Section 3. Then the paper is concluded in Section 4 with a summary and concluding remark.

2. Methods

The whole algorithm consists of 3 parts: the upper-tropospheric moisture retrieval, segmentation, and optimized adjustment.

2.1. Upper-Tropospheric Moisture Retrieval

For the upper-tropospheric moisture retrieval, it is based on the function of the upper-level moisture and brightness temperature of WV channels suggested by Soden and Bretherton [14]. The formula is shown as follows:

$$\ln \left(\frac{RH}{\cos\theta} \right) = a - b \times T_{6.7} \tag{1}$$

where RH is the relative humidity and $T_{6.7}$ is the brightness temperature of WV channel of Fengyun-2E geostationary satellite (the center wave length is 6.7 μm), and θ is the zenith angle of satellite, a and b is the constant numbers.

According to the Clausius-Clapeyron equation, the relative humidity can be rewritten as:

$$RH = q \times \left(\frac{1}{\varepsilon} \times \frac{P_{d0}}{E_s(T_0)} \right) \times \exp \left(-\lambda \frac{T - T_0}{T_0} \right) \tag{2}$$

where q is the moisture mixing ratio, λ is a constant, P_{d0} and T_0 are the reference pressure and temperature in troposphere which are set to 400 hPa and 240 K [15]. $\varepsilon = \frac{R_d}{R_v}$ where $R_d = 287.05 \text{ J}\cdot\text{kg}^{-1}\cdot\text{K}^{-1}$, $R_v = 461.5 \text{ J}\cdot\text{kg}^{-1}\cdot\text{K}^{-1}$ represent the specific gas constant for dry air and moisture respectively.

Based on the above equations, the upper-tropospheric moisture [16] can be written as:

$$q = \exp [c_0 + c_1 (T_{6.7} - \bar{T} - c_2 \times \ln(\cos\theta) + T_0)] \tag{3}$$

where, c_0 , c_1 and c_2 are constants which are set as 5.964, -0.063 and 8.9 respectively. \bar{T} is the weighted average of the temperature at 300 hPa, 400 hPa and 500 hPa. Figure 1 shows the comparison of the original satellite image and its corresponding retrieval specific humidity at upper troposphere by using the above equations. It is noticed that the dark areas in the Water Vapor (WV) channel image (Figure 1a) correspond to the areas with low moisture in the upper-level moisture map (Figure 1b).

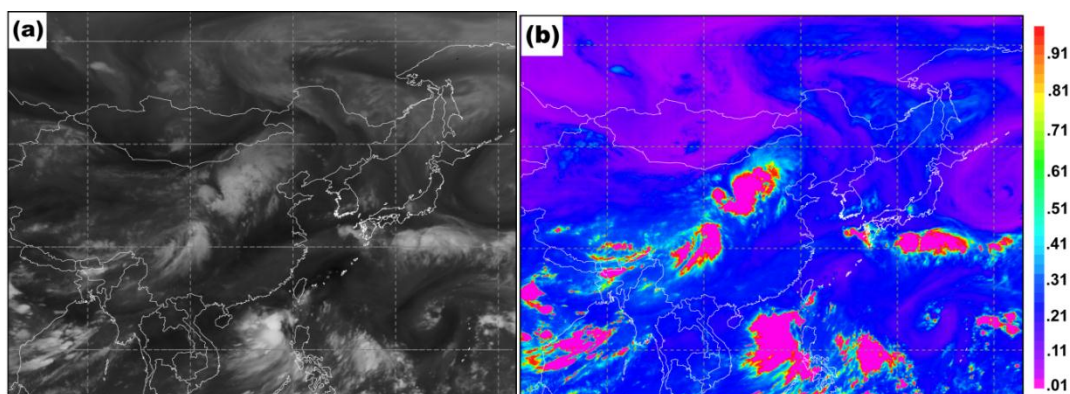


Figure 1. (a) FY2E Water Vapor (WV) channel image at 0000UTC 21 July 2012; (b) the corresponding retrieval specific humidity at upper troposphere ($\text{g}\cdot\text{kg}^{-1}$).

2.2. Segmentation

According to the previous studies, during the course of the air parcels traveling upward to the upper-troposphere/lower-stratosphere the moisture content of the air parcels will decrease. This property makes the moisture as a good tropospheric tracer. On the other hand, it is found that most part of ozone reside in the stratosphere. Therefore ozone is always regarded as a stratospheric tracer. The potential vorticity is considered to be conserved when neglecting friction and diabatic heating. It is often found to have a large value but a small value within stratosphere and troposphere respectively which makes the potential vorticity as a key parameter for detecting dry intrusion from stratosphere. Therefore, based on the results obtained in Section 2.1, the properties of the moisture, ozone and potential vorticity are used together to separate the air from troposphere against that from stratosphere on satellite images in this study.

As documented above, the air parcels are always in the state of non-saturation under the circumstances of rainstorm and some other severe convective weather conditions which means that the air in the dry intrusions associated with those weather conditions could not be completely dry [17]. So the conservation of the Ertel potential vorticity which is only valid for dry air will not be valid under such conditions. While the general moisture potential vorticity which proposed by Gao et al. [18] is proven to have the ability to be generally used for all the conditions by using a condense ratio function in the Ertel potential vorticity equation. The equation is shown as Equations (4) and (5) as follows:

$$\theta^* = \theta \exp \left[\frac{L}{c_p} \frac{q_s}{T} \left[\frac{q}{q_s} \right]^k \right] \tag{4}$$

$$P_m = \alpha \zeta_a \times \Delta\theta^* \tag{5}$$

where P_m is the general moisture potential vorticity, ζ_a is the absolute vorticity, α and $\Delta\theta^*$ are the specific volume and static stability respectively.

Figure 2 shows the moisture distribution as a function of the general moisture potential vorticity and ozone respectively based on the statistics of 3.8 million samples randomly selected from ECMWF Interim dataset covering four seasons in year 2008. The samples of air parcels are grouped into three types which come from troposphere, the mixing zone of troposphere and stratosphere, and the stratospheric areas. The criterion for the classification is based on the Equation (6).

$$\left\{ \begin{array}{ll} H > \tilde{H}_{\max} & (\tilde{H}_{\max} = \max \langle H_d, H_t \rangle) \quad \text{Stratosphere} \\ \tilde{H}_{\min} \leq H \leq \tilde{H}_{\max} & (\tilde{H}_{\max} = \max \langle H_d, H_t \rangle, \quad \tilde{H}_{\min} = \min \langle H_d, H_t \rangle) \quad \text{UT/LS} \\ H < \tilde{H}_{\min} & (\tilde{H}_{\min} = \min \langle H_d, H_t \rangle) \quad \text{Troposphere} < 400 \text{ hPa} \end{array} \right. \tag{6}$$

It can be seen from Figure 2a,c that both the relations between the potential vorticity and moisture and that between ozone and moisture take a “L” pattern and have a small temporal variance which means that a solid negative correlation between these three elements can be found in all year around. Furthermore, a probability distribution analysis is made to get a typical distribution patterns between potential vorticity and moisture and that between ozone and moisture. As shown in Figure 2b,d, the blue dots represent the samples with the probability under 1% and the yellow dots denote those having the probability of 1%–10%. The orange and red dots are those with the probability of 10%–50% and over 50%. A regression is made for those samples having probability over 1%. The regression functions of potential vorticity and moisture and that of ozone and moisture are shown as Equations (7) and (8) respectively (the confidence level of these two regressions are 94% and 88% respectively).

$$Y = 12.40310546 \times e^{(-13.81471572X)} \tag{7}$$

$$Y = -147.4663656 \times \ln(X) - 170.9865546 \tag{8}$$

Based on the regression functions, the moisture threshold for stratospheric air can be set at $0.0808 \text{ g}\cdot\text{kg}^{-1}$. Therefore the dry intrusion from stratosphere can be preliminarily detected on the satellite images.

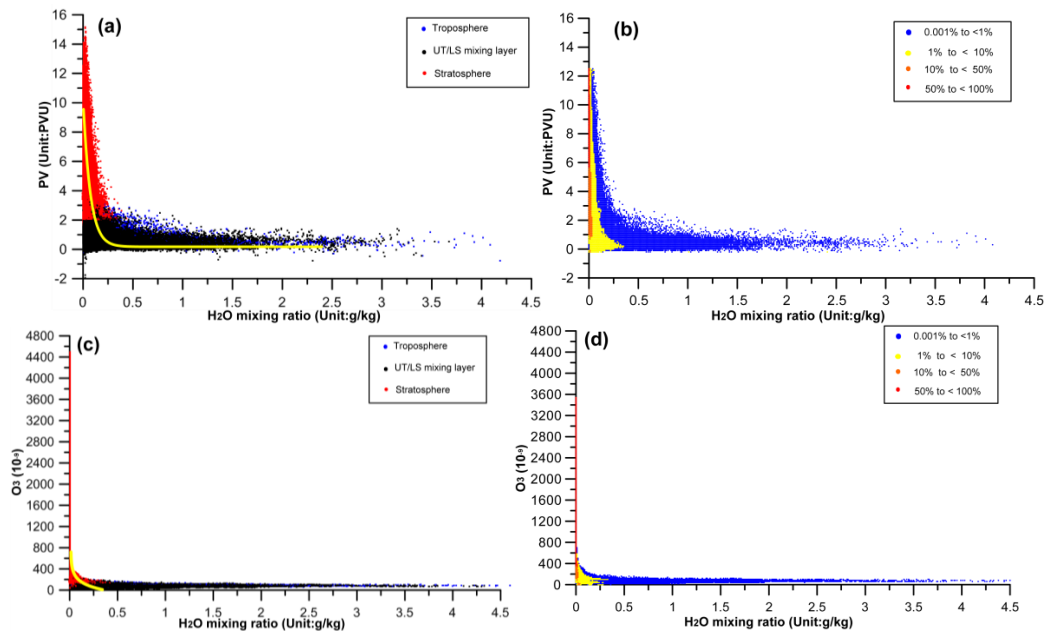


Figure 2. (a,b) Distribution and occurrence probability of the isentropic general moist potential vorticity and moisture from upper troposphere (over 400 hPa) to stratosphere; (c,d) same as (a,b) but for the ozone and moisture. (The red, blue and black points in figure (a,c) indicate air mass come from stratosphere, upper troposphere and mixing area between upper troposphere and lower stratosphere, the yellow curves are the fitting curves; The blue, yellow, orange and red points in figure (b,d) represent air masses occurrence probability lower than 1% and between 1%–10%, 10%–50% and over 50%).

2.3. Optimized Adjustments

To accurately recognize the dry intrusion, two optimized adjustments are used in this study. The first adjustment is to use the climatological dynamic tropopause height. The idea of using climatological dynamic tropopause height is inspired by Bak et al. [19] who use climatological ozone profiles to improve the retrieval of the ozone within upper-troposphere/lower-stratosphere region. Following their idea, the climatological tropopause height is used here to compare with current tropopause height. If an area which is recognized as a dry intrusion area using the above two steps whose current tropopause height is lower than the climatological one, then the area will be kept as a potential dry intrusion area otherwise it would be removed.

It was documented by many studies that dry intrusion has a closed relationship with upper-level jets. Such relationship is first found by Reed [20] during a study of the polar-frontal jets. Based on that, upper-level jets are selected as the second criterion for the optimized adjustment in this study. Although it is known that a dry intrusion is often associated with an upper-level jet, the spatial correlation between them is unknown. Thus a statistical analysis of the spatial correlation of the dry intrusion and upper-level jets is made. Normally, an upper-level jet is axisymmetric system which means we can use its major axis to represent the position of the upper-level jet [12]. To extract the major axis of an upper-level jet a morphological image processing method, One Pass Thinning Algorithm (OPTA) skeleton extraction [21] is used. Figure 3 is shown as an example by using the OPTA skeleton extraction to get the major axes of upper-level jets. It can be seen the locations of upper-level jets are well represented by their axes.

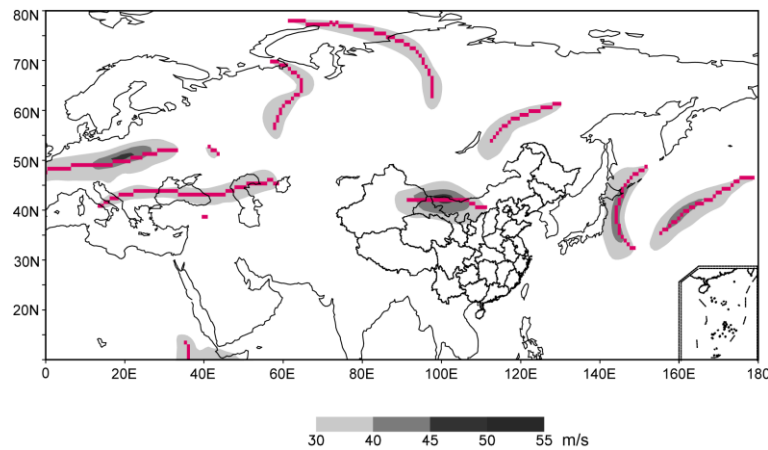


Figure 3. Upper level jets over 350 K isentropic surface (shadings, unit: m s^{-1}) at 0000 UTC 20 July 2012 with their corresponding axes (red solid lines).

Based on that, the occurrence probabilities of the dry intrusion within the range of 0–1000 km away from upper-level jets at 340 K, 345 K, 350 K and 355 K isentropic surfaces are calculated. It is noticed that the mean occurrence probability is about 0.15 while it will increase when the distance is no more than 300 km (Figure 4). By using this criterion, dry intrusions that occurred within 300 km away from upper-level jets will be kept. And the depth of dry intrusion is assigned by the 2PVU isen-potential vorticity surface height.

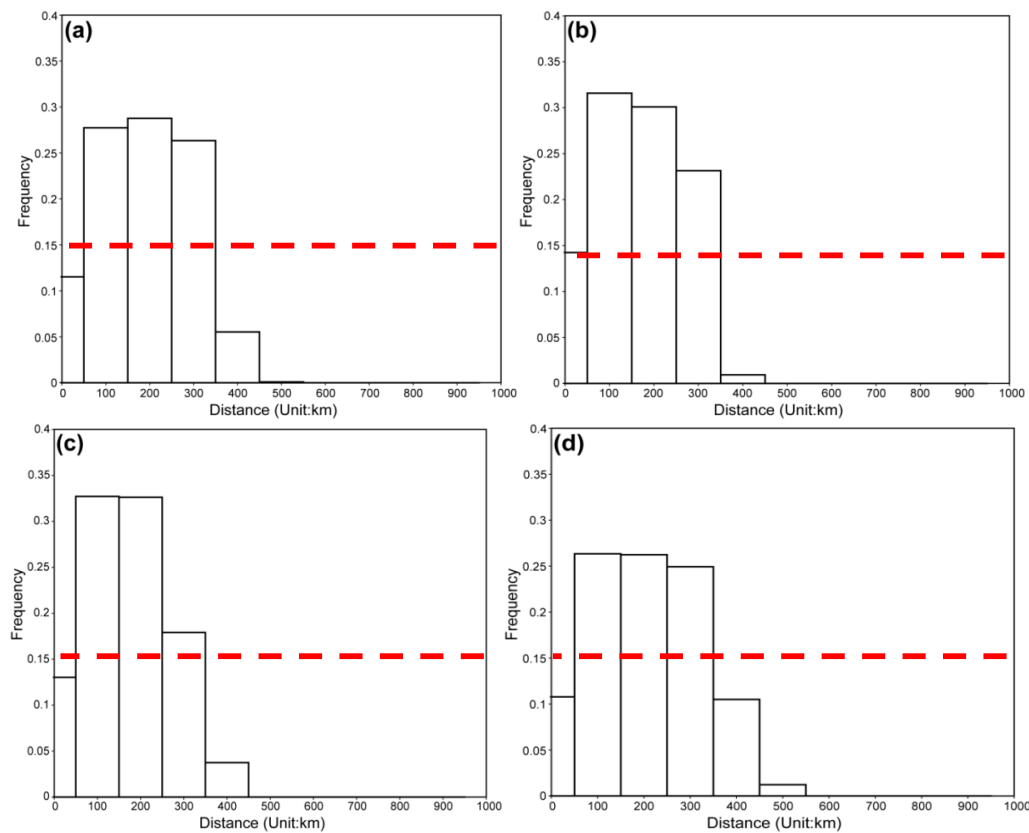


Figure 4. Frequency distribution of distances between dry intrusions and jet axes at 340–355 K isentropic surfaces with 5 K interval ((a) 34 K; (b) 345 K; (c) 350 K; (d) 355 K) (horizontal and vertical coordinate denote distance and frequency distribution correspondingly).

3. Results

3.1. Validation

The new method for detecting dry intrusion described in this study is validated by using some indirect observations. The ozone profiles retrieved from Fengyun-3B are used to validate the dry intrusions. Figure 5 is an example that a dry intrusion is occurred. It can be seen that an elevation of the ozone concentration is occurred at about 200 hPa at (49°N, 108°E) on the ozone profiles retrieved by Fengyun-3B (Figure 5b). The lowest boundary of the dry intrusion estimated by our method at that place is about 350 hPa which is not well consistent with the observation by Fengyun-3B. This discrepancy could be partly owed to the relatively coarse vertical resolution of the ozone profiles retrieved by Fengyun-3B which has only 5 layers below 200 hPa.

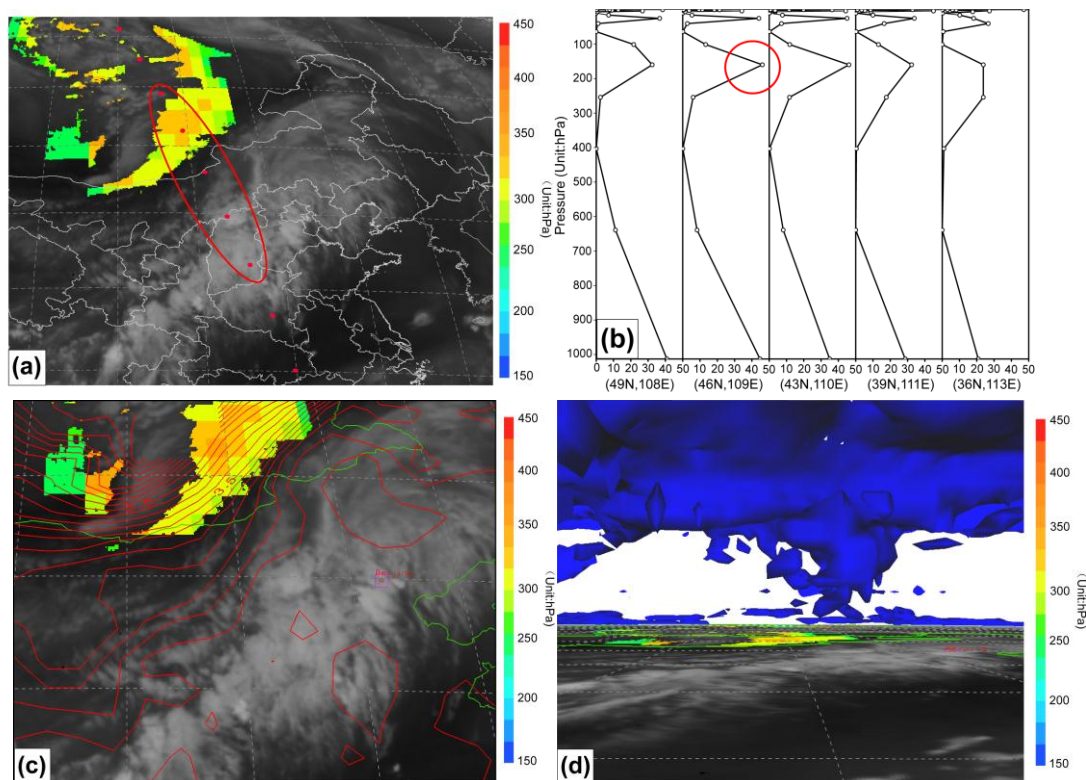


Figure 5. (a) The lowest boundary of dry intrusion (hPa) at 0500UTC 21 July 2012 superimposed with the scanning trace of FY3B Solar Backscatter Ultraviolet Sounder at 0456UTC 21 July 2012 (red points); (b) the ozone profiles (unit: DU(Dobson Unit)) of the 5 points in the red circle in Figure 5a; (c) dry intrusions at 0600 UTC 21 July 2012, with positive potential vorticity at 200 hPa (≥ 2 PVU); (d) 3-dimensional perspective view of dry intrusions at 0600 UTC 21 July 2012 (the blue rendering parts represent the positive vorticity larger than 2 PVU and its vertical range is from 50–1000 hPa).

Another evidence is found on the 3-D potential vorticity map calculated by using NCEP Final Analysis (FNL) data. As Figure 5d shows, a positive potential vorticity column extends from the upper level to the lower level where a dry intrusion is detected. Such structure indicates air parcels from stratosphere penetrate into troposphere over this area.

Since the aim of developing the new algorithm in this study is to detect the dry intrusion related to severe weather processes such as rainstorm and some other convective events, two mid-latitude storm episodes are selected for a further evaluation. The two weather events selected in this study are a heavy rainstorm event occurred in Beijing on 21 July 2012 and a hailstorm event occurred in Zhejiang province in China on 19 March 2014.

3.2. Case I: A Rainstorm Event

The heavy rainstorm (the maximum daily rainfall of 460 mm) event occurred in Beijing on 21 July 2012 is reported as the heaviest rainfall in Beijing since 1950. The rainfall made mud-rock flows and urban waterlog which brought a great loss in human life and property. Figure 6 shows the precipitation during that period. From the figures we can see that the precipitation is concentrated on a small area on the southeast part of the city. Besides, both the variations of the mean and extreme precipitation rate shown as Figure 6b,c suggest that the heavy precipitation (precipitation rate over $50 \text{ mm}\cdot\text{h}^{-1}$) lasted for about 8–9 h during which 4 short-term fluctuations are observed (Figure 6c). These characteristics together indicate that this rainfall event is closed related to meso-scale weather systems.

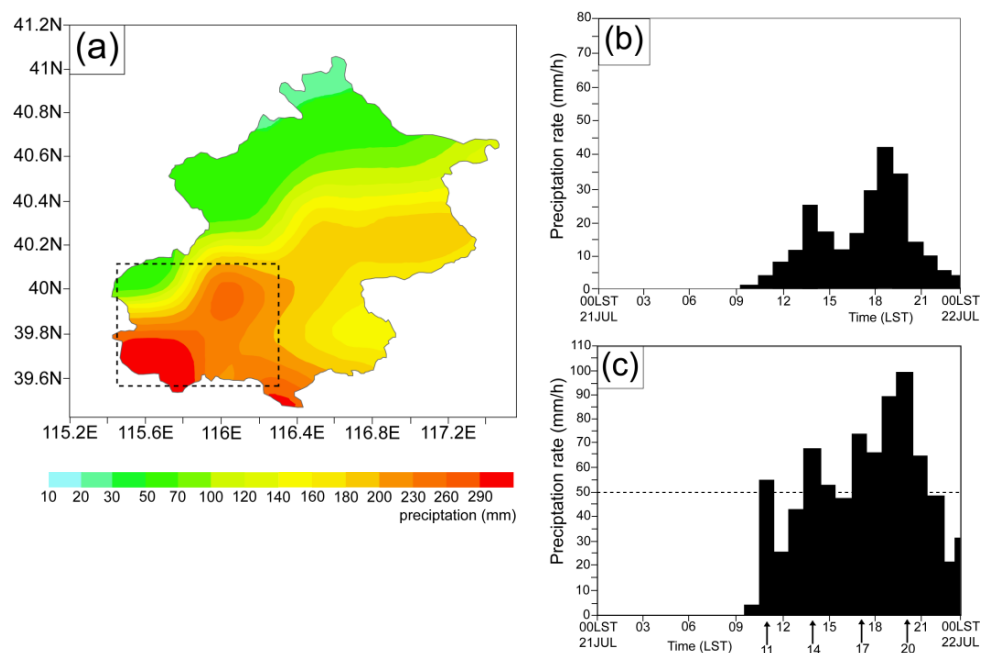


Figure 6. Observed precipitation over Beijing on 21 July 2012. (a) the horizontal distribution of the total rainfall during 08:00 LST 21 July–08:00 LST 22 July 2012 (unit: mm); (b) time evolution of the area-averaged rainfall within the black dash rectangle area in Figure 6a; (c) same as Figure 6b but for the time evolution of the maximum rainfall observed in the dash rectangle area in Figure 6a (Unit: mm).

According to the synoptic features, the rainstorm was occurred accompanied with a synoptic frontal cyclone (not shown). Meanwhile, two tropical storms “Vicente” and “Khanun” generated in the northwest Pacific supplied plenty moisture (over $9 \times 10^{-3} \text{ g}\cdot\text{cm}^{-1}\cdot\text{h}\cdot\text{Pa}^{-1}\cdot\text{s}^{-1}$ [22]) to the precipitation area from south and east. It was noticed that in the earlier stage of the rainfall (before 11:00 LST), although the moisture is plentiful for the precipitation area, the intensity of rainfall is relatively weak (hourly rainfall $\leq 10 \text{ mm}\cdot\text{h}^{-1}$) due to the lack of cold dry air. So to trace the dry air and evaluate their impacts on this rainfall event, the dry intrusion analysis using our new method is made.

Figure 7 shows the time evolution of the dry intrusion during this rainfall event. It can be seen that a region of dry intrusion was occurred to the west of the precipitation area about 12 h before the heavy rainfall occurs (Figure 7a). The maximum of the dry intrusion at that time was located apart from the center of the cold advection. After that this area was observed moving southeastward closed to the center of the cold advection at middle level at 14:00 LST when the rainfall began to increase (Figure 7b). At 20:00 LST when the precipitation reached the maximum, the location of the maximum of dry intrusion was observed to be consistent with that of the cold advection at middle level. In this case, the cold dry air from upper-level was confronted with the warm moist air at lower level thus

inducing a southwest-northeastward rain band (Figure 7c). During the dissipation stage, a split was occurred within the original dry intrusion area. The south part continued moving northeastward accompanied with cold advection at middle level. Thus it can be seen that the occurrence of the dry intrusion is a key factor to trigger the heavy precipitation in this case.

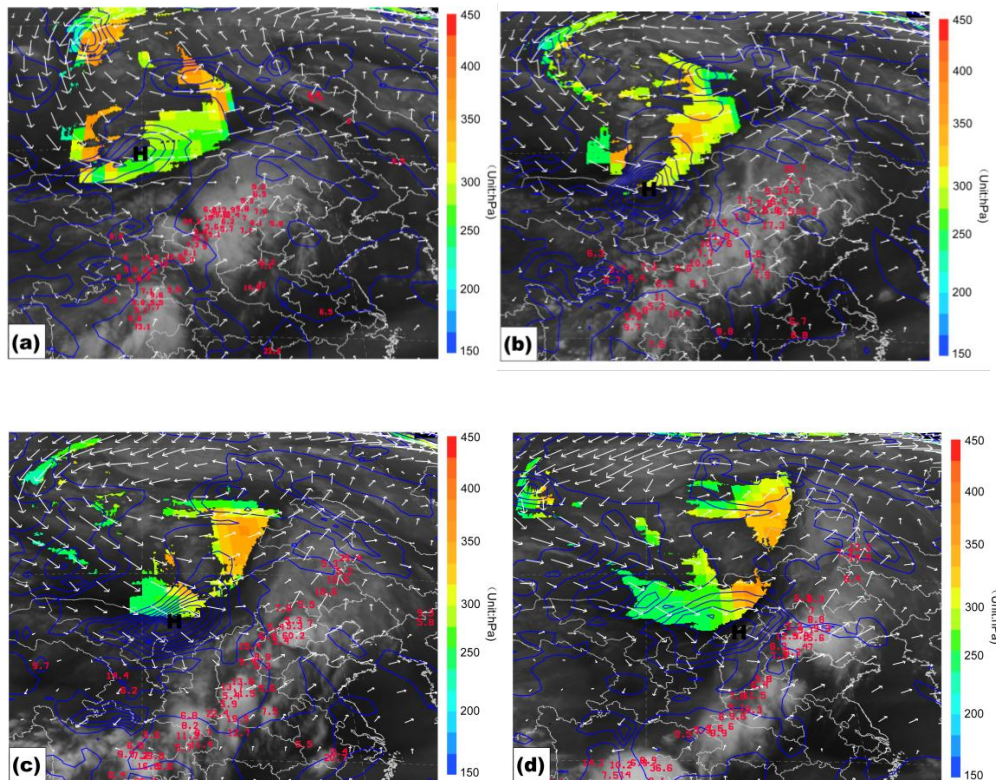


Figure 7. Dry intrusion (color shaded) composited by FY2E WV channel images, cold advection (blue thick line) and wind (white vector) at 320 K isentropic and hourly rainfall (over 5 mm, in red digital) (a) 0800 LST 21 July; (b) 1400 LST 21 July; (c) 2000 LST 21 July; (d) 0200 LST 22 July 2012.

3.3. Case II: Hailstorm Event

Another episode is a hailstorm event which occurred at Taizhou in Zhejiang province of China. Same as the first case, this case is also occurred in front of a cold front. According to the report, a wide spread rainstorm was occurred over Zhejiang, Jiangsu, Anhui and Jiangxi provinces before 16:00 LST 19 March 2014 (Figure 8a). When the raincloud moved eastward over mid-east of Zhejiang at about 16:00 LST, it caused a hailstorm instead of rainstorm over that area. The whole process lasted only 10 min and only a small area of Taizhou city was impacted by this hailstorm. Although it has a short life term and quite regional the photos shown in Figure 8b suggest that the intense of the hailstorm is high (the diameter of hails was reported to be bigger than 2.5 cm). So far, radar observations are widely used to monitor such kind of convective events. Nevertheless, forecasters still find difficulty in forecasting such kind of system since it is occurred in a small region during a short term. Therefore, it is curious to know if there are any other signs such as dry intrusions from upper-level troposphere can provide an early warning for such disastrous weather event.

Figure 9 shows the WV channel image superimposed by the positive vorticity and dry intrusions 24 h before the hailstorm. It can be seen that an unobvious dry intrusion was occurred over southwest to north part of Zhejiang province with the lowest intrusion boundary reaching 400 hPa over southeast part. To verify it, the skew T log-P diagram (a plot of vertical profile of the temperature and dew point through the atmosphere above a certain point on the ground) at the maximum of this dry intrusion is examined. It is encouraging to note that there are two dry layers locating at 150 hPa and 400 hPa

respectively (Figure 8b) which suggests that the dry intrusion depth is well estimated. As documented by many studies [23,24], large quantity of energy is needed for the development of severe convective systems. CAPE and DCAPE which are two energy indices are usually used for measuring the energy related to convective systems. CAPE is the convective available potential energy which often indicates the intensity of the upward motion while DCAPE is the maximum energy available to a descending air parcel. Normally the higher the value of CAPE (DCAPE) is, the stronger the convection (downdraft) potential will be. It is shown that the CAPE and DCAPE over Taizhou at 16:00 LST 18 March 2014 is about 0 and 300 J·kg⁻¹ respectively which means both the convection at low-level and dry intrusion from upper-level are weak.

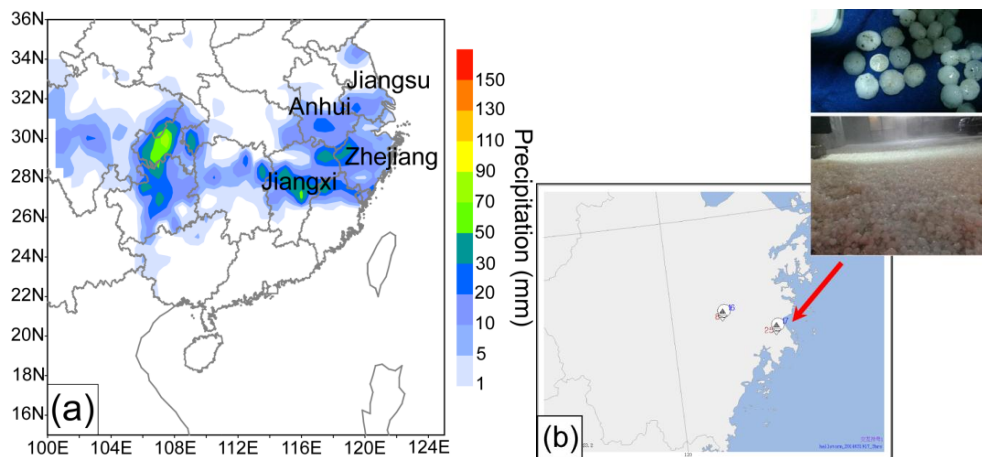


Figure 8. (a) The 24-hr accumulated rainfall on 19 March 2014. (b) Hailstorms observed at Taizhou city in Zhejiang province of China.

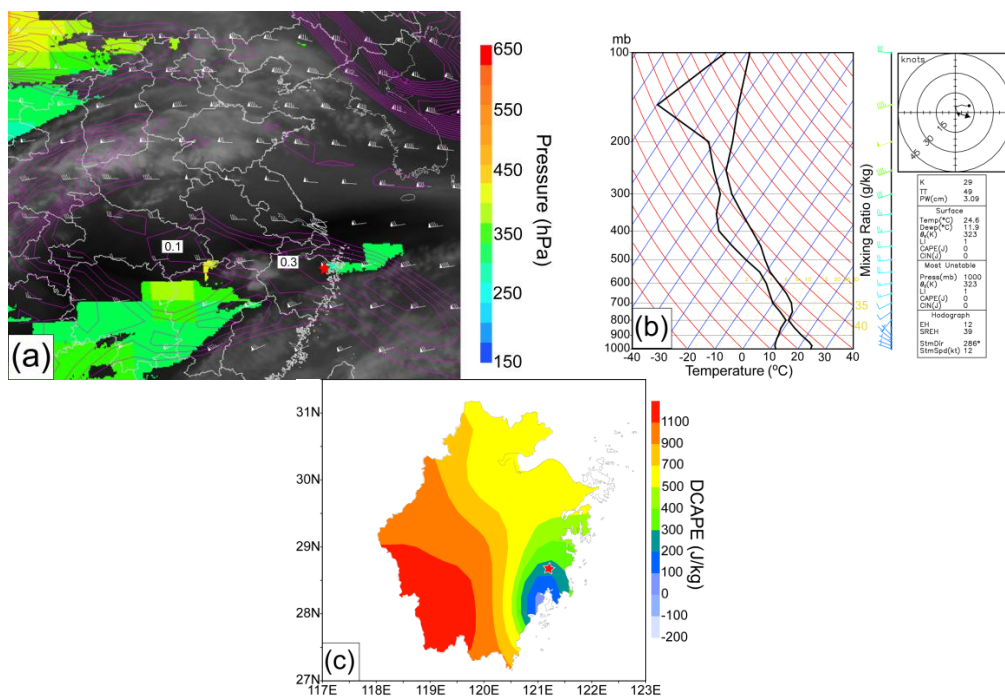


Figure 9. (a) The composition map of dry intrusion (shadings) and positive vorticity (contours, unit: 10⁻⁴ s⁻¹) at 315 K isentropic layer at 16:00 LST 18 March 2014. (b) skew T log-P diagram at the location shown with starisk in Figure 8a; (c) DCAPE distribution within Zhejiang province (The starisk denotes the location of Taizhou city) (Unit: J·kg⁻¹).

While 12 h later (not shown), it is found both the area and intensity of the dry intrusion over north part of Zhejiang increase. The lowest boundary of the dry intrusion reached to about 550 hPa which was consistent with the position of dry layers observed in the skew T log-P diagram. Besides, the CAPE and DCAPE at that time increased to $400 \text{ J}\cdot\text{kg}^{-1}$ and $400 \text{ J}\cdot\text{kg}^{-1}$ respectively. Figure 10 shows the distribution of dry intrusion 6 h before the hailstorm. Although a decrease in the dry intrusion area over Zhejiang province was found, the lowest boundary of the dry intrusion reached to about 700 hPa. Meanwhile, the positive vorticity at 315 K isentropic layer was observed increasing beneath the intrusion area with the maximum reached $0.5 \times 10^{-4} \text{ s}^{-1}$. The DCAPE was also experienced a sharp increase and got nearly $1000 \text{ J}\cdot\text{kg}^{-1}$ while the CAPE was still maintained at $400 \text{ J}\cdot\text{kg}^{-1}$ during this period. Typically, DCAPE values over $800 \text{ J}\cdot\text{kg}^{-1}$ are often statistically significant and imply downward transport of higher momentum air to the surface. According to Hoskins’s PV view [25], a high positive abnormal of PV transported downward by dry intrusion will increase positive vorticity which will trigger the development of a meso-scale cyclone at the lower level. Therefore, from this perspective, dry intrusion may be a major contributor to the development of this hailstorm in Zhejiang. As expected, the dry intrusion disappeared when the hailstorm occurred (not shown). And when the hailstorm ceased, both the CAPE and the DCAPE dropped steeply with the DCAPE value being of $200 \text{ J}\cdot\text{kg}^{-1}$. Based on the above, we can see that the temporal and spatial variations of dry intrusion match with the hailstorm quite well. The early appearance of the dry intrusion over the hailstorm area can be seen as a pre-warning of such kind of convective weather.

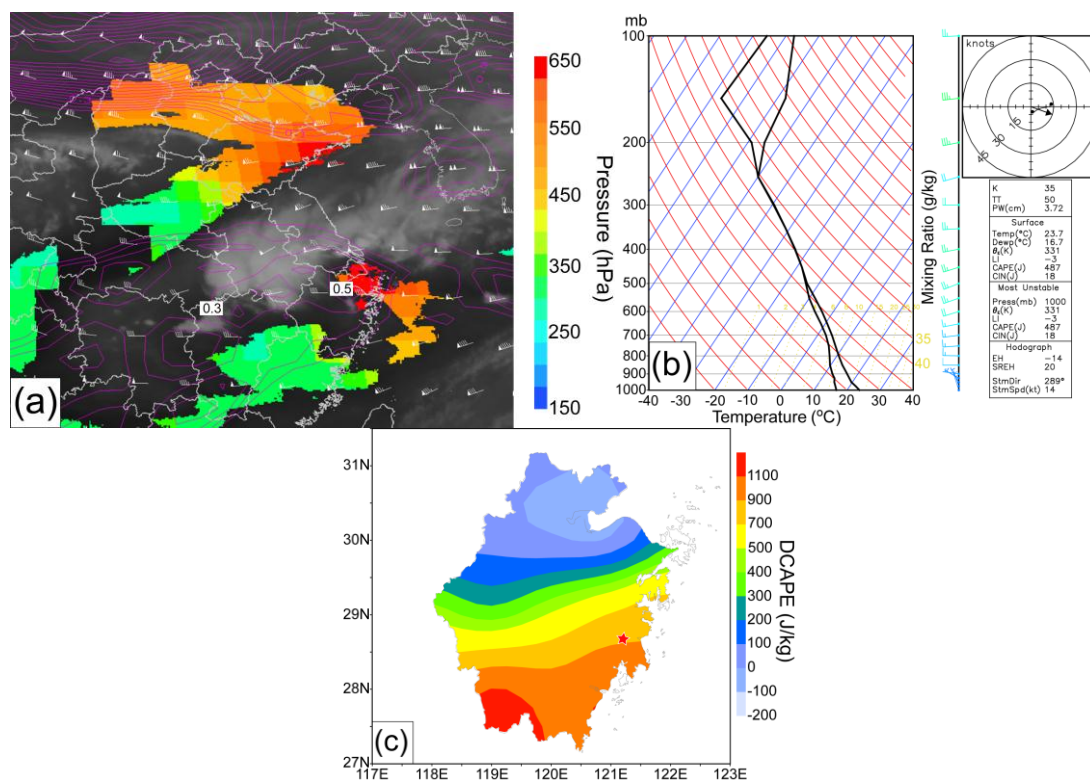


Figure 10. (a) The composition map of dry intrusion(shadings) and positive vorticity (contours, unit: 10^{-4} s^{-1}) at 315 K isentropic layer at 10:00 LST 19 Mar 2014. (b) skew T log-P diagram at the location shown with starisk in Figure 9a; (c) DCAPE distribution within Zhejiang province (The starisk denotes the location of Taizhou city).

4. Conclusions

Dry intrusion is an important phenomenon within the upper-troposphere and lower-stratosphere region. It is significant for the troposphere-stratosphere exchange, severe precipitation and some

other disastrous weather. Due to its importance, several methods for detecting this phenomenon are set up. So far the methods of combining diagnosis and modeling are widely used and proven to be more efficient. However, all of them are built on the basis of the hypothesis of the dry atmosphere. This hypothesis to some extent will limit the range of the applications especially for those related to convective weather episodes. Therefore, an improved method considering the moisture effect by using a general moisture potential vorticity is set up.

In this method, statistical analyses are made to acquire the relation between satellite-retrieved upper-level moisture and modeling general moist potential vorticity and ozone. The method is tested by using Fengyun-2E satellite and ECMWF Interim data and validated by using Fengyun-3B observed ozone profiles and NCEP FNL analysis data. Two mid-latitude disastrous weather episodes occurred in China in 2012 and 2014 are selected as demonstration to show the applicability of the method we developed in this study. Actually except for these two cases occurred in the mid-latitude areas of China, this method is also tested on some other places in the rest of the mid-latitude globe (e.g., Europe) by using different data. For example, we made a preliminary test on a rainstorm event occurred in UK during 30–31 July 2006 by using MSG-SEVIRI (Spinning Enhanced Visible and Infrared Imager of Meteosat Second Generation) data. In that case a dry intrusion was observed at the upstream area of UK and the temporal and spatial variations of that dry intrusion are found to have a good agreement with the rainfall either. Although those tests over the rest of the mid-latitude globe look encouraged, more validations of the results are needed due to the limits of observations.

Based on the above, the method proposed in this study for detecting dry intrusions related to mid-latitude storm looks reasonable and applicable. It can be used in analyzing the mid-latitude convective weather episodes and can be a supplementary index for helping forecaster to make a pre-warning for those weather events if a more detailed statistics of the temporal and spatial relations between dry intrusion and severe weather are made.

For future works, we consider to test the algorithm on more cases around the world under different circumstances including considering those weather episodes occurred around some special landforms such as large mountain ranges and continental/ocean boundaries.

Acknowledgments: This work was supported by the Chinese National Science Founding (NSFC) grants 41575048 and 41175023.

Author Contributions: In this work, Yi-Xuan Shou and Feng Lu set up the entire algorithm and performed the experiments; Shaowen Shou contributes to the meteorological analysis of the disastrous weather events.

Conflicts of Interest: The authors declare no conflict of interest.

References

1. Shou, S.; Li, S.; Yao, X. *Mesoscale Meteorology*; Meteorological Press: Beijing, China, 2003. (In Chinese)
2. Reid, H.J.; Vaughan, G. Convective mixing in a tropopause fold. *Q. J. R. Meteorol. Soc.* **2004**, *130*, 1195–1212. [[CrossRef](#)]
3. Nastrom, G.D.; Green, J.L.; Gage, K.S.; Peterson, M.R. Tropopause folding and the variability of the tropopause height as seen by the flatland VHF radar. *J. Appl. Meteorol.* **1989**, *28*, 1271–1281. [[CrossRef](#)]
4. Bertin, F.; Campistron, B.; Caccia, J.L.; Wilson, R. Mixing processes in a tropopause folding observed by a network of ST radar and Lidar. *Ann. Geophys.* **2001**, *19*, 953–963. [[CrossRef](#)]
5. Roger, B.W.; Holmes, S.J. Water vapor imagery: Interpretation and applications to weather analysis and forecasting. *NOAA Tech. Rpt. NESDIS* **1991**, *57*, 213.
6. Lamarque, J.F.; Hess, P.G. Cross-tropopause mass exchange and potential vorticity budget in a simulated tropopause folding. *J. Atmos. Sci.* **1994**, *51*, 2246–2269. [[CrossRef](#)]
7. Bithell, M.; Gray, L.J.; Cox, B.D. A three-dimensional view of the evolution of midlatitudes stratospheric intrusions. *J. Atmos. Sci.* **1999**, *56*, 673–688. [[CrossRef](#)]
8. Appenzeller, C.; Davies, H.C. Structure of stratospheric intrusions into the troposphere. *Nature* **1992**, *358*, 570–572. [[CrossRef](#)]

9. Wimmers, A.J.; Moody, J.L.; Browell, E.V.; Hair, J.W.; Grant, W.B.; Butler, C.F.; Fenn, M.A.; Schmidt, C.C.; Li, J.; Ridley, B.A. Signatures of tropopause folding in satellite imagery. *J. Geophys. Res.* **2003**, *108*, 8360. [[CrossRef](#)]
10. Moody, J.L. Tropopause folding at satellite-observed spatial gradients: 1. Verification of an empirical relationship. *J. Geophys. Res.* **2004**, *109*. [[CrossRef](#)]
11. Moody, J.L. Tropopause folding at satellite-observed spatial gradients: 2. Development of an empirical model. *J. Geophys. Res.* **2004**, *109*. [[CrossRef](#)]
12. Michel, Y.; Bouttier, F. Automated tracking of dry intrusions on satellite water vapour imagery and model output. *Q. J. R. Meteorol. Soc.* **2006**, *132*, 2257–2276. [[CrossRef](#)]
13. Michel, Y. Data assimilation of tropopause height using dry intrusion observations. *Mon. Weather Rev.* **2010**, *138*, 101–122. [[CrossRef](#)]
14. Soden, B.J.; Bretherton, F.P. Interpretation of TOVS water vapor radiances in terms of layer-average relative humidities: Method and climatology for the upper, middle, and lower troposphere. *J. Geophys. Res.* **1996**, *101*, 9333–9343. [[CrossRef](#)]
15. Soden, B.J.; Bretherton, F.P. Upper tropospheric relative humidity from the GOES 6.7 μm channel: Method and climatology for July 1987. *J. Geophys. Res.* **1993**, *98*, 16669–16688. [[CrossRef](#)]
16. Moody, J.L.; Wimmers, A.J.; Devenport, J.C. Remotely sensed specific humidity: Development of a derived product from the GOES Imager Channel 3. *Geophys. Res. Lett.* **1999**, *26*, 59–62. [[CrossRef](#)]
17. Gao, S.; Zhou, F.F. Water vapour potential vorticity and its applications in Tropical cyclones. *Chin. Phys. Lett.* **2008**, *25*, 3830–3833.
18. Gao, S.; Wang, X.; Zhou, Y. Generation of generalized moist potential vorticity in a frictionless and moist adiabatic flow. *Geophys. Res. Lett.* **2004**, *31*, 59–62. [[CrossRef](#)]
19. Bak, J.; Liu, X.; Wei, J.C.; Pan, L.L.; Chance, K.; Kim, J.H. Improvement of OMI ozone profile retrievals in the upper troposphere and lower stratosphere by the use of a tropopause-based ozone profile climatology. *Atmos. Meas. Tech. Discuss.* **2013**, *6*, 4333–4369. [[CrossRef](#)]
20. Reed, R.J. A study of characteristic type of upper level frontogenesis. *J. Meteor.* **1955**, *12*, 226–237. [[CrossRef](#)]
21. Wu, J.; Zhang, G.; Xia, J.; Cui, Z. Research on cerebral aneurysm detection based on OPTA algorithm. In Proceedings of the 2009 International Symposium on Information Processing (ISIP'09), Huangshan, China, 13–16 April 2009.
22. Wen, Y.; Xue, L.; Li, Y.; Wei, N.; Lü, A. Interaction between Typhoon Vicente (1208) and the western Pacific subtropical high during the Beijing extreme rainfall of 21 July 2012. *J. Meteor. Res.* **2015**, *29*, 293–304. [[CrossRef](#)]
23. Kuchera, E.L.; Parker, M.D. Severe convective wind environments. *Wea. Forecast.* **2006**, *21*, 595–612. [[CrossRef](#)]
24. Schlatter, P.T.; Schlatter, T.W.C.; Knight, A. An unusual hailstorm on 24 June 2006 in Boulder, Colorado. Part I: Mesoscale setting and radar features. *Mon. Wea. Rev.* **2008**, *136*, 2813–2832. [[CrossRef](#)]
25. Hoskins, B.J. Towards a PV- θ view of the general circulation. *Tellus* **1991**, *43*, 27–35.

